Transactions of the Materials Research Society of Japan 29 [8] 3659-3664 (2004)

Order-N Algorithm for Linear Response Function

Toshiaki Iitaka
RIKEN (The Institute of Physical and Chemical Research)
2-1 Hirosawa, Wako, Saitama 351-0198, Japan.
e-mail:tiitaka@riken.jp URL: http://atlas.riken.jp/~iitaka

We review recent development of algorithm for linear response functions of quantum systems described by a very large Hamiltonian matrix. These numerical methods are combinations of numerical solution of the time-dependent Schroedinger equation, random vector representation of trace, and Chebyshev polynomial expansion of Fermi- and Boltzmann-operators, whose application includes optical absorption of nanocrystallites, and electron spin resonance (ESR) spectrum of one dimensional antiferromagnets at finite temperature.

I. INTRODUCTION

Computational physicists often face to problems of calculating the linear response functions or the real-time Green's functions of quantum manybody systems with degree of freedom $N \sim 10^6$ or more. Direct diagonalization of the Hamiltonian matrix is the most naive and powerful method for modest system size $N \leq 10^3$. However, it becomes prohibitive for larger system because the computational time grows as N^3. Therefore efficient numerical methods, such as Quantum Monte Carlo methods, Lanczos Methods, and Kernel Polynomial Methods have been developed and applied to various problems.

Quantum Monte Carlo methods (QMC)[1, 2] can generate the Green's functions of very large systems since QMC does not need to store the wave functions. They have been successfully used for evaluating the imaginary-time Green's functions and, therefore, various thermodynamic quantities. However, for evaluating dynamical quantities such as AC conductivity, one has to rely on numerical analytic continuation (e.g. *Maximum Entropy Method* [3]) to obtain the real-time Green's function from the imaginary-time one. This procedure is not straightforward because the statistical errors are amplified by numerical analytical continuation and the default model for the MEM must be assumed *a priori*.

Lanczos Methods (LM)[4, 5] have been useful techniques for evaluating dynamical responses of relatively large systems. The LM uses Lanczos recursion formula with Matrix Vector Multiplications (MVM), $|\phi'\rangle = H|\phi\rangle$, to tridiagonalize the Hamiltonian matrix, which leads to a continued fraction representation of the real-time Green's function. The drawback of LM is numerical instability for large numbers of MVM's, which originates in the algorithm. Recently, LM was extended to finite temperatures (Finite Temperature LM, FTLM) by introducing random sampling over the ground and excited eigenstates [6]. However, FTLM has a weak point that the number of excited eigenstates to be calculated increases rapidly as temperature or system size becomes large. Therefore reduction of computational costs by exploiting symmetries of the system becomes crucial.

Kernel Polynomial Method (KPM)[7, 8] calculates density of states and linear response functions by using Chebyshev polynomial expansion [9–11] of broadened delta functions. The Chebyshev polynomials are obtained through Chebyshev recursion formula by using MVM's. Unlike Lanczos recursion, Chebyshev recursion is free from the numerical instability observed in Lanczos recursion even for large numbers of MVM's. The use of KPM for linear response functions has been limited to the ground state calculation.

Time-Dependent method [12] is one of the most efficient and direct methods for calculating the real-time Green's functions and linear response functions, and has been successfully applied to electric conductivities of amorphous arroys, specific heat of quantum spins, etc.

Fermi-Weighted Time-Dependent Method (FWTDM) [13, 14] is a combination of time-dependent method, random vector representation of trace [15], and Chebyshev polynomial expansion of step function $\theta(E_f - H)$ to extract occupied and unoccupied one-particle states of noninteracting fermi particles in the ground state. This method was successfully applied to optical absorption of silicon and carbon nano-crystallites[14].

Boltzmann-Weighted Time-Dependent Method (BWTDM)[16], calculates linear response functions at finite temperatures by using the Boltzmann-weight operator. The BWTDM has an advantage to FTLM that the computational time does not increase as temperature increases, because BWTDM does not calculate any eigenstates at all. Therefore BWTDM does not need use of symmetries and can easily treat disordered systems.

II. TIME-DEPENDENT SCHRÖDINGER EQUATION

With the increasing availability of high performance computers, the development of efficient numerical methods [17, 18] of the time-dependent Schroedinger equation (TDSE) [19]

$$i\frac{d}{dt}|\phi,t\rangle = H|\phi,t\rangle \tag{1}$$

has become an important task in various fields of physics such as scattering theory, quantum chaos, laser-atom/molecule interaction and so on. In this section, we study numerical methods for calculating TDSE with a time-independent Hamiltonian H represented by an $N \times N$ Hermitian matrix and a wave function $|\phi, t\rangle$ represented by N-dimensional complex vector. The atomic units $\hbar = m_e = e = 1$ are used throughout this article. The eigenstates of the Hamiltonian are denoted as

$$H|E_m\rangle = E_m|E_m\rangle, \quad (m = 1, 2, \cdots, N) \tag{2}$$

wile the range of energy spectrum is defined as

$$\Delta E_{grid} = E_{max} - E_{min}, \tag{3}$$

where $E_{max} = \max[\{E_m\}]$ and $E_{min} = \min[\{E_m\}]$ are the largest and smallest eigenvalues of H. Here we define the normalized Hamiltonian by shifting the origin of energy and rescaling the unit of energy.

$$H_{norm} = \frac{H - (E_{max} + E_{min})/2}{(E_{max} - E_{min})/2} \tag{4}$$

which has the eigenvalues in the range of $[-1, +1]$. Hereafter we use H_{norm} in place of H, and write it simply as H by omitting the subscript.

The formal solution of (1) is expressed by the time-evolution operator, i.e., the matrix exponential function [19]

$$|\phi, t + \Delta t\rangle = \exp(-iH\Delta t)\,|\phi, t\rangle \tag{5}$$

Various schemes have been proposed to approximate this exponential function [20–22]. The simplest scheme called Euler scheme (EU) expands the exponential function to the first order of $H\Delta t$,

$$|\phi, t + \Delta t\rangle = (1 - iH\Delta t)|\phi, t\rangle + O((H\Delta t)^2), \tag{6}$$

and uses (6) repeatedly to obtain $|\phi, t + n\Delta t\langle$. This is an explicit scheme, which does not need matrix inversion, but it is numerically unstable due to the lack of the time reversal symmetry ($t \rightarrow -t$). Moreover it is not unitary.

To avoid this instability, the Crank-Nicholson scheme (CN) has been widely used in which the exponential function is approximated by the Caley transform

$$|\phi, t + \Delta t\rangle = \frac{(1 - iH\Delta t/2)}{(1 + iH\Delta t/2)}|\phi, t\rangle + O((H\Delta t)^3), \tag{7}$$

This scheme is unitary, unconditionally stable, and accurate up to $(H\Delta t)^2$. However, this implicit method is prohibitive when the band width of the Hamiltonian is large because the memory and CPU time for solving the linear equation increases as $O(N^2)$. Therefore the development of explicit stable integration methods has been desired.

One of these explicit methods is the Suzuki-Trotter scheme [21, 23].

Another is the symmetrized version of the EU, which is called the second order differencing scheme (MSD2) [22],

$$|\phi, t + \Delta t\rangle - |\phi, t - \Delta t\rangle = -2iH\Delta t|\phi, t\rangle + O((H\Delta t)^3) \tag{8}$$

This scheme is symmetric in time and shown to be conditionally stable [22]. Furthermore, the scheme is accurate up to $(H\Delta t)^2$.

The more accurate and stable method is the Chebyshev scheme (CH) [20]. This method is classified as a global propagator method. It uses very long time steps and sometimes completes the calculation with a single time step.

The CH is very accurate and the error can be reduced up to the machine precision. The only shortcoming of the CH is that the intermediate wave functions are not available, while the stepwise methods, such as the CN and the MSD2, produce the wave function at each time step.

Let us study the stability and error of the various schemes by computing the time-evolution of the eigenstates $|E_m\rangle$. Note that (6-8) contain only unit matrix and Hamiltonian matrix. Therefore, preparing the initial wave function as one of the eigenstates, the wave function remains in the same eigenstates during the time evolution. Then we define the growth factor g as

$$|E_m, t + \Delta t\rangle = g|E_m, t\rangle \tag{9}$$

where g is a complex number. The exact time-evolution should give the growth factor as

$$g = \exp(-iE_m\Delta t) \tag{10}$$

However, an approximate scheme will give the growth factor of general form

$$g = |g| \exp(-iE_m\Delta t + i\epsilon_{phase}). \tag{11}$$

If $|g| \neq 1$ then the scheme becomes numerically unstable and the error in norm grows up exponentially as $|g|^{N_{step}} - 1$, where N_{step} is the number of time steps. If $|g| = 1$ then the norm is conserved and the accumulating error appears only in the phase error ϵ_{phase}. Note that phase error accumulates after N_{step} time evolutions as

$$\epsilon_{phase}(t = N_{step}\Delta t) = \epsilon_{phase}(t = \Delta t)N_{step} \tag{12}$$

which does not growy exponentially but linearly in time. Therefore phase error can be regarded as the error in eigenenergy.

The growth factor equation for EU is obtained by introducing (9) in to (6), $g + i\Delta t - 1 = 0$, where Δt is the dimensionless time step. Then EU is found unconditionally unstable for a finite time step $\Delta t > 0$, $|g| = \sqrt{1 + (\Delta t)^2} > 1$.

The growth factor equation of CN becomes $g = \frac{1 - i\Delta t/2}{1 + i\Delta t/2}$, and CN is found unconditionally stable for any Δt $|g| = 1$

The growth factor equation for MSD2 becomes $g^2 + 2i\Delta t g - 1 = 0$ whose solutions are $g_\pm = -i\Delta t \pm \sqrt{1 - \Delta t^2}$ If and only if the stability condition $|\Delta t| \leq 1$ is satisfied, the scheme is stable $|g_\pm| = 1$.

The phase error under the stability condition can be estimated by the Taylor expansion of the time-evolution operators in (7) and (8),

$$\epsilon_{phase}^{CN} = \frac{1}{12}(\Delta t)^3 N_{step} \tag{13}$$

$$\epsilon_{phase}^{MSD2} = -\frac{1}{6}(\Delta t)^3 N_{step} \tag{14}$$

III. RANDOM VECTOR

A *uniform random vector* is defined by

$$|\Phi\rangle \equiv \sum_{n=1}^{N} |n\rangle \xi_n \tag{15}$$

where $\{|n\rangle\}$ is the basis set used in the computation and ξ_n are a set of random variables generated by a subroutine, which satisfy the statistical relation

$$\langle\langle\ \xi_n\ \rangle\rangle\ =\ 0 \tag{16}$$

$$\langle\langle\ \xi^*_{n'}\xi_n\ \rangle\rangle\ =\ \delta_{n'n}. \tag{17}$$

Here $\langle\langle\ \cdot\ \rangle\rangle$ stands for the statistical average.

This random vector may be also expressed by the eigenstates of H,

$$|\Phi\rangle = \sum_{n=1}^{N} |E_n\rangle \zeta_n. \tag{18}$$

Although we do not know the actual value of ζ_n and $|E_n\rangle$, we can derive the statistical relation of ζ_n as follows.

$$\zeta_n\ =\ \sum_{l=1}^{N} \langle E_n|l\rangle \xi_l \tag{19}$$

$$\zeta^*_n\ =\ \sum_{l=1}^{N} \xi^*_l \langle l|E_n\rangle. \tag{20}$$

Then the statistical relation of ζ_n is derived as

$$\langle\langle\ \zeta_n\ \rangle\rangle\ =\ \sum_{l=1}^{N} \langle E_n|l\rangle\ \langle\langle\ \xi_l\ \rangle\rangle = 0 \tag{21}$$

$$\langle\langle\ \zeta^*_{n'}\zeta_n\ \rangle\rangle\ =\ \sum_{l'=1}^{N}\sum_{l=1}^{N} \langle l'|E_{n'}\rangle\langle E_n|l\rangle\ \langle\langle\ \xi^*_{l'}\xi_l\ \rangle\rangle$$

$$=\ \sum_{l=1}^{N} \langle E_n|l\rangle\langle l|E_{n'}\rangle = \langle E_n|E_{n'}\rangle = \delta_{n'n} \tag{22}$$

We can easily notice that the random vector contains all eigenstates of the Hamiltonian with equal probability. Therefore the random vector (15) represents the system at a very high temperature.

The statistical average of $\langle\Phi|X|\Phi\rangle$ gives the trace of X as follows:

$$\langle\langle\ \langle\Phi|X|\Phi\rangle\ \rangle\rangle\ =\ \sum_{n} \langle E_n|X|E_n\rangle \tag{23}$$

$$+\sum_{n,n'} \langle\langle\ \zeta^*_{n'}\zeta_n - \delta_{n'n}\ \rangle\rangle\ \langle E_{n'}|X|E_n\rangle$$

$$=\ \sum_{n} \langle E_n|X|E_n\rangle = \mathrm{tr}\,[X] \tag{24}$$

in the eigenstate basis representation.

The second term in (23) gives the statistical fluctuation when the statistical average is evaluated by using random vectors. The order of the fluctuation is estimated as follows[24]: Assuming all non-zero matrix elements have the value of order 1, the first term in (23) becomes order of N, while the second term becomes order of $\sqrt{N}$ for sparce matrices because the the number of non-zero matrix elements is order N for sparce matrices and the order of fluctuation is proportional to the square root of it. As a result, the relative statistical error will be order of $\sqrt{N}/N = 1/\sqrt{N}$. For example, the statistical error becomes order of 10^{-3} for $N = 10^6$, which can be considered as small. If the statistical fluctuation is not small enough with a set of random vectors, the calculation can be repeated with M sets of random vectors for reducing the fluctuation to order of $1/\sqrt{MN}$. When the spectral density such as DOS and linear response function, the dimension of matrix N in the above estimation should be replaced by N_{eff}, the number of resonaces with in the spectral resolution η, e.g. $N_{eff} = \rho(\omega)\eta$ in case of DOS. Therefore to reach the same accuracy we need more random vectors for higher energy resolution or low temperatures. See Ref. [15] for more sophisticated analysis of this statistical fluctuation.

Next, we try to simulate the Fermi degenerated ground state of a non-interacting many-electron system by a single one-particle wave function, and use this wave function to calculate the linear-response function of the system. We define a *projected random vector* by applying the projection operator $\theta(E_f - H)$ to the random vector,

$$|\Phi_{E_f}\rangle \equiv \theta(E_f - H)|\Phi\rangle. \tag{25}$$

The projected random vector may be also expressed by the basis set $\{|E_n\rangle\}$,

$$|\Phi_{E_f}\rangle = \sum_{E_n \le E_f} |E_n\rangle \zeta_n \tag{26}$$

where E_f is the Fermi energy. Then the statistical average of $\langle\Phi_{E_f}|X|\Phi_{E_f}\rangle$ gives the sum of contributions from each occupied states

$$\langle\langle\ \langle\Phi_{E_f}|X|\Phi_{E_f}\rangle\ \rangle\rangle$$

$$=\ \sum_{E_n \le E_f} \langle E_n|X|E_n\rangle = \mathrm{tr}[\theta(E_f - H)X] \tag{27}$$

Boltzmann-weighted random vectors, $|\Phi_{Boltz}\rangle = e^{-\beta H/2}|\Phi\rangle$, and numerical solution of the time-dependent Schrödinger equation.

IV. CHEBYSHEV POLYNOMIAL

Function of matrix H, f(H), can be expanded by Chebyshev polynomials [11],

$$f(H)|\phi\rangle = \sum_{n=0}^{N_{CH}} a_n T_n(H)|\phi\rangle \tag{28}$$

where $T_n(x)$ are the Chebyshev polynomials of n-th order, and a_n are the expansion coefficients.

In the case of $f(H) = \exp(-iHt)$, $a_0 = J_0(t)$ and $a_n = 2(-i)^n J_n(t), (n > 0)$ [9, 25] where $J_n(x)$ is the

Bessel function of the first kind. The order of Chebyshev expansion N_{CH} is taken large enough to obtain good convergence.

In the case of $f(H) = \exp(-\beta H)$, $a_0 = I_0(\beta)$ and $a_n = 2I_n(\beta), (n > 0)$ [9] where $I_n(x)$ is the modified Bessel function of the first kind.

In the case of $f(H) = \theta(E_f - H)$, $a_0 = 1 - \phi_f/\pi$ and $a_n = 2g_m \sin(m\phi_f)/m\pi, (n > 0)$ where g_m is the damping factor [26]

The Chebyshev polynomial of n-th order $T_n(x)$ is calculated by the Chebyshev recursion formula,

$$T_{n+1}(H)|\phi\rangle = 2HT_n(H)|\phi\rangle - T_{n-1}(H)|\phi\rangle. \quad (29)$$

V. NANO-CRYSTALLITE

In this section we introduce the Projection Method for linear-response function . First we review a simple derivation of the linear-response function by using full many-body state. Second we introduce the *projected random vector*, which simulates the ground states of a non-interacting many-electron system by a single one-particle wave function. Then, combining these two concepts, we derive a fast algorithm for the linear-response function of a non-interacting many-electron system.

The linear-response $\delta B(t)$ to an impulse of perturbation $A\delta(t)$ forced on a quantum system described by the Hamiltonian H is calculated as

$$\delta B(t) = 2\,\mathrm{Im}\langle\phi^{(0)}|e^{+iHt}Be^{-iHt}A|\phi^{(0)}\rangle \quad (30)$$

and the Fourier transformation of $\delta B(t)$ gives the linear response to the perturbation $Ae^{-i\omega t}$

$$\chi_{BA}(\omega + i\eta) = \int_0^T dt\; e^{+i(\omega+i\eta)t}\delta B(t) \quad (31)$$

where the imaginary part of frequency η is introduced to limit the integration time to a finite value $T = -\ln\delta/\eta$ with δ being the relative numerical accuracy of Eq. (31).

By introducing the projected random vector (26) into $|\phi^{(0)}\rangle$ in (30) and then into (31), we obtain our final result, i.e., the linear response of a non-interacting many-electron system,

$$\chi_{BA}(\omega + i\eta) = \left\langle\!\!\left\langle \int_0^T dt\; e^{+i(\omega+i\eta)t}\delta B(t) \right\rangle\!\!\right\rangle \quad (32)$$

where $\delta B(t)$ represents the sum of the response from each electron below the Fermi energy, which is defined by

$$\delta B(t) = 2\,\mathrm{Im}\langle\Phi_{E_f}|e^{+iHt}Be^{-iHt}\theta(H - E_f)A|\Phi_{E_f}\rangle. \quad (33)$$

In (33), another projection operator $\theta(H - E_f)$ has been introduced to ensure that the excited states should be higher than the Fermi energy.

For calculating (32) and (33), we start with one realization of the random vector (15), and calculate two wave functions,

$$|\phi^{(0)};t\rangle = e^{-iHt}|\Phi_{E_f}\rangle \quad (34)$$

$$|\delta\phi;t\rangle = e^{-iHt}\theta(H - E_f)A|\Phi_{E_f}\rangle \quad (35)$$

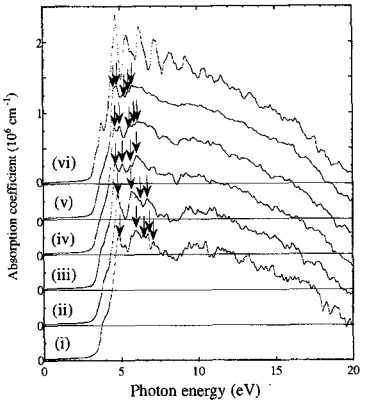

FIG. 1: Optical absorption coefficient of hydrogenated Si nanocrystallites (i) $Si_{1050}H_{498}$, (ii) $Si_{1632}H_{666}$, (iii) $Si_{4048}H_{1182}$, (iv) $Si_{8120}H_{1950}$, and (v) $Si_{13464}H_{2730}$ and (vi) bulk Si with 13824 Si atoms. Zero points of the y-axis are shifted as shown by the horizontal lines. Several peak positions are denoted by the arrows[28].

where the time evolution is calculated by the leap frog method [17] and the projection operators are calculated by the Chebyshev polynomial expansion [13, 27]. At each time step, the response (33) and its Fourier transformation (32) are evaluated. Since the leap frog method and the Chebyshev polynomial expansion consist of the matrix-vector operation $H|\phi\rangle$ whose computational efforts are of Order(N) for sparse Hamiltonians, the total computational effort also becomes of Order(N).

Figure 1 shows the calculated absorption coefficient spectra given by $K = 2\omega k/c$ with the complex refractive index defined by $n + ik = \varepsilon^{1/2}$[28].

VI. NANO-MOLECULAR MAGNET

In this section, we apply BWTDM to study Electron Spin Resonance spectrum of one-dimensional $s = \frac{1}{2}$ antiferromagnet Cu benzoate $Cu(C_6H_5COO)_2 \cdot 3H_2O$, especially the dynamical crossover between *spinon* excitation and *breather* excitation as a function of temperature. Nonperturbative analytical calculation of this phenomena is a very difficult problem which still open. Even within Sine Gordon theory, the linear response functions have been studied only at high temperature regime (by perturbation) and at zero temperature. We compare our numerical results with preceding experimental and theoretical studies [29–39].

The effective Hamiltonian of one-dimensional $s = \frac{1}{2}$ antiferromagnet Cu benzoate may be written [36–38] as

$$H = \sum_{j=1}^{N_{spin}} \left[J\mathbf{s}_j \cdot \mathbf{s}_{j+1} - g\mu_B H_x s_j^x + (-1)^j g\mu_B hs_j^y \right] \quad (36)$$

The first term is the isotropic Heisenberg antiferromagnet where $\mathbf{s}_j$ is spin operator at the j-th site, $J/k_B = 17.2K = 1.48(meV)$ is the exchange interaction [29],

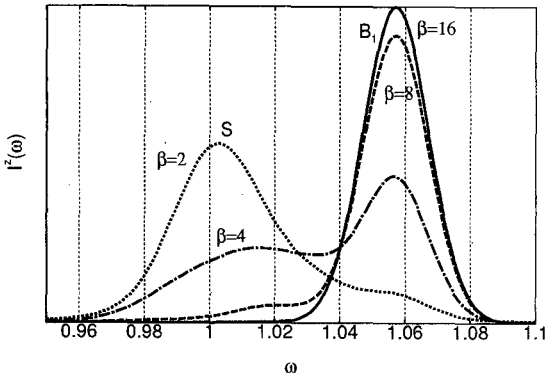

FIG. 2: ESR spectra of normal polarization, $I^z(\omega)$, calculated with $\beta = 2 \sim 16$, $H_x = 1.0$, $N_{spin} = 16$, $\eta = 0.01$ and $N_{rand} = 16$. S and B_1 stand for spinon excitation and first breather excitation, respectively.

and the sums are taken over N_{spin} spins with periodic boundary conditions. The second is the normal Zeeman term due to the external uniform magnetic field H_x. The third is the staggered Zeeman term due to induced staggered magnetic field $h = 0.065H_x$ originating from the Dzyaloshinskii-Moriya (DM) interaction and the staggered component of the g tensor[34]. In the following we assume that $g = 2.25(2.29)$ with H_x along $c(c'')$-direction. Unit of magnetic field and frequency become $J/g_c\mu_B = 11.4(T)$, $J/g_{c''}\mu_B = 11.2(T)$, and $J/h = 359(GHz)$, respectively.

According to the linear response theory, absorption of electromagnetic waves of frequency ω and polarization μ is expressed as

$$I^{\mu}(\omega) = \frac{H_R^2 \omega}{2} \chi''_{\mu\mu}(q=0,\omega) \tag{37}$$

where H_R is the amplitude of the electromagnetic waves and $\chi''_{\mu\mu}(q,\omega)$ is the imaginary part of the dynamical magnetic susceptibility,

$$\chi''_{\mu\mu}(q,\omega) = (1-e^{-\beta\omega}) \, \mathrm{Im} \lim_{\eta\to+0} \int_0^{\infty} dt e^{-i(\omega-i\eta)t} g_q^{\mu}(t) \tag{38}$$

at inverse temperature $\beta = 1/(k_B T)$. The correlation function is defined by

$$g_q^{\mu}(t) = \mathrm{Tr}\left[e^{-\beta H} M_{-q}^{\mu} e^{+iHt} M_{+q}^{\mu} e^{-iHt}\right] / \mathrm{Tr}\left[e^{-\beta H}\right] \tag{39}$$

where the magnetization operator is $M_q^{\mu} = \sum_{j=1}^{N_{spin}} s_j^{\mu} \frac{e^{iqj}}{\sqrt{N_{spin}}}$.

The essence of BWTDM is evaluation of eq. (39)

$$g_q^{\mu}(t) = \frac{\langle\langle \langle \Phi_{Boltz}|M_{-q}^{\mu} e^{+iHt}|M_{+q}^{\mu}|e^{-iHt}|\Phi_{Boltz}\rangle \rangle\rangle}{\langle\langle \langle \Phi_{Boltz}|\Phi_{Boltz}\rangle \rangle\rangle} \tag{40}$$

by using *Boltzmann-weighted random vectors*, $|\Phi_{Boltz}\rangle = e^{-\beta H/2}|\Phi\rangle$, and numerical solution of the time-dependent Schrödinger equation.

In real calculation, we first generate N complex random numbers ξ_n and construct $|\Phi\rangle$ according to eq. (15). The $|\Phi_{Boltz}\rangle$ can be computed with numerical stability by applying eq. (28) repeatedly to $|\Phi\rangle$. Then $\langle\Phi_{Boltz}|\Phi_{Boltz}\rangle$ gives a sample of the denominator of eq. (40). Here, we introduce another vector $|\Phi_{M_{+q}^{\mu}}\rangle = M_{+q}^{\mu}|\Phi_{Boltz}\rangle$ and calculate the time evolution of $|\Phi_{Boltz}\rangle$ and $|\Phi_{M_{+q}^{\mu}}\rangle$ by eq.(8). At each time $t = n\Delta t$, the matrix element $\langle\Phi_{M_{+q}^{\mu}}; t|M_{+q}^{\mu}|\Phi_{Boltz}; t\rangle$ gives a sample of numerator of eq. (40). After calculating the denominator and numerator for N_{rand} random vectors, the ratio of their averages gives $g_q^{\mu}(t)$ of eq. (40). Then $\chi''_{\mu\mu}(q,\omega)$ with a finite frequency resolution η is calculated by using Gaussian filter,

$$\chi''_{\mu\mu}(q,\omega) = (1-e^{-\beta\omega}) \, \mathrm{Im} \int_0^{T_{max}} dt e^{-i\omega t} g_q^{\mu}(t) \left[A e^{-\eta^2 t^2/2}\right] \tag{41}$$

where T_{max} is related to η by $T_{max} \sim \eta^{-1}$. In order to avoid finite size effect of spinon excitations, T_{max} is chosen so that $T_{max} < N_{spin}/v_{spin}$ where $v_{spin} \sim 1$ is the spin wave velocity [38]. This limits the finest frequency resolution. Note that this is not the limit due to the algorithm but due to the finite size model. Much finer resolution can be used for breather modes, which are spatially localized.

Figure 2 shows the ESR spectra of normal polarization (Faraday configuration) $I^z(\omega)$ calculated with various temperatures. At high temperatures ($\beta \leq 5$), S is outstanding in the spectrum, and its peak shifts to higher frequency and becomes broadened as temperature decreases while B_1 becomes narrower. At low temperatures ($\beta \geq 5$), B_1 prevails while its peak frequency is almost constant and its width becomes much smaller than the numerical resolution η. This crossover behavior between spinon excitation and first breather excitation has become computable by the invention of BWTDM, and the result is consistent with both experimental [30] and field-theoretical results [34]. Several other weak peaks appear in our results as well as in experimental results, which are supposed to be higher-order breathers and transitions between excited states. However, we are not going to analyze them here.

In summary, we developed an efficient and stable algorithm for linear response functions at finite temperatures, and studied the ESR spectra of $s = \frac{1}{2}$ antiferromagnet Cu benzoate for a wide range of temperature and magnetic field. We reproduced experimental results of the spinon-breather crossover as a function of temperature. Temperature dependence of the width and shift of the peaks are also calculated, which are consistent with experiments and analytical theories. The calculated frequency of B_1 as a function of H_x agrees well with both experimental and field-theoretical results at low fields, and reproduces the deviation of experimental results from the Sine Gordon theory at high fields, where the low energy assumption of the Sine Gordon theory may be broken and the choice of the compactification radius R becomes ambiguous[35]. The advantage of BWTDM is being applicable to finite temperatures, strong magnetic field and high frequency while its weak point is

finite size effects ($N_{spin} \leq 20$). The computational cost of BWTDM is moderate. Calculation of one curve in Fig. 1, for example, requires approximately 30 minutes with 8 CPU's of Fujitsu VPP5000 vector-parallel computer.

acknowledgments

The results presented here were computed by using supercomputers at RIKEN and NIG.

[1] M. Suzuki, S. Miyashita, and A. Kuroda. *Prog. Theor. Phys.*, 58:1377, 1977.
[2] W. Linden. *Phys. Rep.*, 220:53, 1992.
[3] R.N. Silver, J.E. Gubernatis, and D.S. Sivia. *Phys. Rev. Lett.*, 65:496, 1990.
[4] C. Lanczos. *J. Res. Nat. Bur. Stand.*, 45:255, 1950.
[5] E. Dagotto. *Rev. Mod. Phys.*, 66:763, 1994.
[6] J. Jaklic and P. Prelovsek. *Phys. Rev. B*, 49:5065, 1994.
[7] R. N. Silver and H. Roeder. *Int. J. Mod. Phys. C*, 5:735, 1994.
[8] L. W. Wang and A. Zunger. Solving schroedinger's equation around a desired energy: Application to silicon quantum dots. *J. Chem. Phys.*, 100(3):2394, 1994.
[9] R. Kosloff and H. Tal-Ezer. *Chem. Phys. Lett.*, 127:223, 1986.
[10] W. Kunishima, T. Tokihiro, and H. Tanaka. Error estimation of recursive orthogonal polynomial expansion method for large hamiltonian system. *Comp. Phys. Commun.*, 148:171–181, 2002.
[11] W. H. Press, S. A. Teukolsky, W. T. Vetterling, and B. P. Flannery. *Numerical Recipes in Fortran 77*. Cambridge University Press, 1994.
[12] M. L. Williams and H. J. Maris. *Phys. Rev. B*, 31:4508, 1985.
[13] T. Iitaka, S. Nomura, H. Hirayama, X Zhao, Y. Aoyagi, and T. Sugano. O(n) algorithm for linear response functions of non-interacting electrons. *Phys. Rev. E*, 56:1222, 1997.
[14] S. Nomura, T. Iitaka, X. Zhao, Y Aoyagi, and T Sugano. Linear scaling calculation for optical-absorption spectra of large hydrogenated silicon nanocrystallites. *Phys. Rev. B*, 56(8):R4348, 1997.
[15] A. Hams and H. De Raedt. Fast algorithm for finding the eigenvalue distribution of very large matrices. *Phys. Rev. E*, 62:4365, 2000.
[16] T. Iitaka and T. Ebisuzaki. Algorithm for linear response functions at finite temperatures: Application to esr spectrum of $s = \frac{1}{2}$ antiferromagnet cu benzoate. *Phys. Rev. B*, 90:047203, 2003.
[17] T. Iitaka. Solving the time-dependent schrodinger equation numerically. *Phys. Rev. E*, 49:4684, 1994.
[18] Toshiaki Iitaka. *Introduction to Quantumdynamics*. Parity Physics Course. Maruzen, Tokyo, 1994.
[19] J.J. Sakurai. *Modern Quantum Mechanics (revised version)*. Addison Wesley, Massachusetts, 1994.
[20] C. Leforestier, R.H. Bisseling, C. Cerjan, M.D. Feit, R. Friesner, A. Guldberg, A. Hammerich, G. Jolicard, W. Karrlein, H.-D. Meyer, N. Lipkin, O. Roncero, and R. Kosloff. *J. Comp. Phys.*, 94:59, 1991.
[21] H. De Raedt. *Comp. Phys. Rep.*, 7:1, 1987.
[22] A. Askar and A.S. Cakmak. *J. Chem. Phys.*, 68(6):2794, 1978.
[23] M. Suzuki. *Phys. Lett. A*, 146:319, 1990.
[24] T. Iitaka. Computing the real-time green's functions of large hamiltonian matrices. *High Performance Computing in RIKEN*, 1995. (physics/9802021).
[25] A. Vijay and H. Metiu. *J. Chem. Phys.*, 116:60, 2002.
[26] R. N. Silver, H. Roeder, A. F. Voter, and J. D. Kress. *J. Comp. Phys.*, 124:115, 1996.
[27] O. F. Sankey, D. A. Drabold, and A. Gibson. Projected random vectors and the recursion method in the elecronic-structure problem. *Phys. Rev. B*, 50:1376, 1994.
[28] S. Nomura, T. Iitaka, X. Zhao, , T. Sugano, and Y. Aoyagi. Quantum size effect in model nanocrystalline/amorphous mixed-phase silicon structures. *Phys. Rev. B*, 59(15):10309, 1999.
[29] K. Oshima, K. Okuda, and M. Date. *J. Phys. Soc. Jpn.*, 44:757, 1978.
[30] T. Asano it et al. *Phys. Rev. Lett.*, 84:5880, 2000.
[31] A. Ogasahara. S. Miyashita. *Prog. Theor. Phys. Suppl*, 145:286, 2002.
[32] M. Oshikawa and I. Affleck. *Phys. Rev. Lett.*, 82:5136, 1999.
[33] I. Affleck and M. Oshikawa. *Phys. Rev. B*, 60:1038, 1999.
[34] M. Oshikawa and I. Affleck. *Phys. Rev. B*, 65:134410, 2002.
[35] M. Oshikawa. *Prog. Theor. Phys. Suppl.*, 145:243, 2002.
[36] M. Oshikawa and I. Affleck. *Phys. Rev. Lett.*, 79:2883, 1997.
[37] F. H. L. Essler and A. M. Tsvelik. *Phys. Rev. B*, 57:10592, 1998.
[38] F. H. L. Essler. *Phys. Rev. B*, 59:14376, 1999.
[39] J. Lou it et al. *Phys. Rev. B*, 65:064420, 2002.

(Received October 11, 2003; Accepted March 4, 2004)